Permeability of the windows of the brain: Feasibility of dynamic contrast-enhanced MRI of the circumventricular organs

Inge C.M. Verheggen (inge.verheggen@maastrichtuniversity.nl)
Maastricht University https://orcid.org/0000-0001-7749-5994
Joost J.A. de Jong
Maastricht University Medical Center
Martin P.J. van Boxtel
Maastricht University
Alida A. Postma
Maastricht University Medical Center
Frans R.J. Verhey
Maastricht University
Jacobus F.A. Jansen
Maastricht University Medical Center
Walter H. Backes
Maastricht University Medical Center

Research

Keywords: Circumventricular organs, dynamic contrast-enhanced magnetic resonance imaging, permeability, pharmacokinetic modeling

Posted Date: October 16th, 2020

DOI: https://doi.org/10.21203/rs.3.rs-46100/v3

Version of Record: A version of this preprint was published on October 28th, 2020. See the published version at https://doi.org/10.1186/s12987-020-00228-x.

Abstract

Background: Circumventricular organs (CVOs) are small structures without a blood-brain barrier surrounding the brain ventricles that serve homeostasic functions and facilitate communication between the blood, cerebrospinal fluid and brain. Secretory CVOs release peptides and sensory CVOs regulate signal transmission. However, pathogens may enter the brain through the CVOs and trigger neuroinflammation and neurodegeneration. We investigated the feasibility of dynamic contrast-enhanced (DCE) MRI to assess the CVO permeability characteristics in vivo, and expected significant contrast uptake in these regions, due to blood-brain barrier absence.

Methods: Twenty healthy, middle-aged to older males underwent brain DCE MRI. Pharmacokinetic modeling was applied to contrast concentration time-courses of CVOs, and in reference to white and gray matter. We investigated whether a significant and positive transfer from blood to brain could be measured in the CVOs, and whether this differed between secretory and sensory CVOs or from normal-appearing brain matter.

Results: In both the secretory and sensory CVOs, the transfer constants were significantly positive, and all secretory CVOs had significantly higher transfer than each sensory CVO. The transfer constants in both the secretory and sensory CVOs were higher than in the white and gray matter.

Conclusions: Current measurements confirm the often-held assumption of highly permeable CVOs, of which the secretory types have the strongest blood-to-brain transfer. The current study suggests that DCE MRI could be a promising technique to further assess the function of the CVOs and how pathogens can potentially enter the brain via these structures.

Trial registration: Netherlands Trial Register number: NL6358, date of registration: 2017-03-24

1. Background

1.1. The circumventricular organs

The circumventricular organs (CVOs) are structures located adjacent to the third and fourth ventricles of the brain (1-3). An important characteristic of these structures is that they have extensive and highly permeable capillaires that lack a blood-brain barrier (BBB). The vessels in the CVOs branch into a network of fenestrated capillaries with loosely connected astrocytic endfeet (Figure 1). As a consequence, substances can travel freely between the blood and the CVO tissue, making neurons more susceptible to peripheral signals (4). The CVOs contain ependymal cells called tanycytes that have apical processes that extend into the cerebrospinal fluid (CSF) to monitor CSF composition and distal processes that contact the fenestrated capillaries to control the exchange of substances between the blood and CSF (1, 4-6). The tanycytes contain tight junction proteins (Figure 1). Although a barrier between the vasculature and brain tissue is missing, these tight junctions form a barrier guarding the ventricular components and controlling the diffusion of blood-borne substances to the CSF (7). The CVOs are considered as points of

communication between the blood, CSF and brain parenchyma and, in general, serve to maintain homeostasis (6, 8).

1.2. Functions of the circumventricular organs

The CVOs can be divided in two groups: secretory and sensory types (Figure 1). The secretory CVOs include the neurohypophysis (NH), median eminence (ME) and pineal gland (PG) (1, 5). The secretory CVOs are involved in hormone and peptide secretion, neurochemical transport and chemoreception (5) (Table 1). The sensory CVOs include the subfornical organ (SFO), organum vasculosum of the lamina terminalis (OVLT) and area postrema (AP) (5).

The sensory CVOs can sample molecules from the blood and brain interstitial fluid and pass this information on to other brain structures. They have connections with major neural effector centers for most autonomic functions and have important roles in sodium and water balance, cardiovascular regulation, energy metabolism and immunomodulation (1, 9) (Table 1). The sensory CVOs allow communication between the endocrine, immune and central nervous system and thereby contribute to body fluid homeostasis (4). For example, angiotensin, a hormone regulating vasoconstriction, arterial pressure and cardiovascular function, acts through signaling into the sensory CVOs (10). Via their action on CVOs, pharmacotherapy such as angiotensin blockers can decrease blood pressure and cardiovascular morbidity (11).

The subcommissural organ (SCO) is sometimes considered to be a CVO, due to its extensive communication with the CSF (2). However, the SCO does not have a large network of fenestrated capillaries (5), which is an essential feature of the CVOs, and therefore, we did not include the SCO as a CVO.

The CVOs also play a role in inflammation as they can be entry points for inflammatory cells and are involved in cytokine secretion (12, 13). The immune system communicates with the brain to activate the hypothalamic-pituitary-adrenal-axis (HPA-axis) (14). This communication involves activation of the CVOs, which subsequently secrete pro-inflammatory cytokines. Many disorders, such as depression, schizophrenia and Alzheimer's disease (AD), are associated with disruption of the HPA-axis (15). Investigating the connection between the CVOs and HPA-circuits may lead to the detection of abnormalities at early stages of disease (4).

Studies in sheep have demonstrated that blood-borne prions can enter the central nervous system (CNS) via the CVOs (16, 17). Prion accumulation is linked to chronic inflammation in prion disease. Prion accumulation occurs in the CVOs, from where the infection can spread to other brain areas. When pathogens enter through the CVOs, they can activate a cytokine-transcription cascade which produces prostaglandins, subsequently leading to more widespread BBB disruption and CNS pathology (4).

The CVOs have thus been linked to neuroinflammation and characteristics of neurodegenerative disorders and may be involved in neurotoxic protein accumulation. More knowledge on the CVOs could possibly help in the detection of abnormalities at early stages of disease, as they may be the first place for neurotoxins to accumulate, or offer a new pharmaceutical target not hampered by the BBB.

1.3. Imaging techniques for the circumventricular organs

Finding a feasible method to visualize the CVOs is an important first step in gaining more in vivo knowledge on these rather small structures and their role in disease etiology. Since the CVOs do not have a BBB, a contrast agent is expected to transfer rapidly from the blood plasma into the brain tissue. Previous studies have used post-gadolinium enhancement brain MRI to assess CVO visibility (5, 18). In the current study, we use brain images obtained with a dynamic contrast-enhanced (DCE) MRI technique, which can detect dynamic concentration changes of intravenously administered gadolinium contrast-agent, to investigate whether it is feasible to assess the permeability properties of the CVOs. This DCE MRI technique uses a dual-time resolution protocol, which makes our measurements susceptible to both the early rapid temporal changes capturing the vascular component and the later slower features to capture contrast agent extravasation (i.e. permeability) (19).

1.4. Research question

Our main hypothesis states that significant and positive gadolinium-based contrast agent transfer will be detected in the CVO tissue, due to the absence of the BBB. Additionally, we investigated whether permeability in the secretory CVOs differed from that in the sensory CVOs, and whether permeability in the CVOs differed from the permeability measured in the normal-appearing brain matter. Moreover, cerebral blood flow, which influences blood-to-brain transfer (20, 21), is known to decrease during aging (22). Therefore, we investigated whether the contrast enhancement in the CVOs was age-dependent.

Table 1: Short overview of the characteristics of the circumventricular organs

	Type	Location	Size [mm]	Primary function	Hormones	Ref.
NH	Secretory	Posterior part of the hypophysis originating from the floor of the third ventricle	1.0 – 2.9	Releasing hormones received from the paraventricular and supraoptic nuclei	Vasopressin Oxytocin	(2, 23)
ME	Secretory	Extension of the floor of the third ventricle	0.3	Hypophysial portal system: transporting hormones to the hypophysis	Vasopressin Oxytocin	(2, 24)
PG	Secretory	Posterior wall of the third ventricle	1.7	Regulating circadian rhythms	Melatonin	(2, 6)
OVLT	Sensory	Rostral wall of the third ventricle	0.2	Water and sodium homeostasis and immune response	Angiotensin II Cytokines	(2, 4, 6)
SFO	Sensory	Inferior surface of the fornix/ roof of the third ventricle	0.3 – 0.6	Water and sodium homeostasis	Angiotensin II	(2, 6)
AP	Sensory	Floor of the fourth ventricle	0.5	Opening the central canal, cardiovascular and respiratory regulation and controlling the vomiting center	Substance P	(2, 4, 6)

Abbreviations: NH = neurohypophysis; ME = median eminence; PG = pineal gland; SFO = subfornical organ; OVLT = organum vasculosum of the lamina terminalis; AP = area postrema.

2. Materials And Methods

2.1. Participants

Recently, a follow-up on a subsample of participants of the Maastricht Aging Study (MAAS) (25) was conducted, in which 61 individuals who had shown no evidence of cognitive or functional decline were included (Mini-Mental State Examination score ³ 25; Disability Assessment for Dementia score > 90%; no diagnosis of dementia, mild cognitive impairment or other psychiatric or neurological disorders; no structural brain abnormalities; no cognitive impairment due to substance abuse). All participants provided written informed consent before participation. For the current study, we used the imaging data of the 10 youngest (median age = 53.5 years, age range = 47 - 56) and the 10 oldest (median age = 73.5 years, age range: 70 - 91) male participants (Additional file 1, Table 1.1.). Previous studies have

demonstrated that the estrous cycle influences CVO activity (26-28), so only male individuals were included in this feasibility study.

2.2. MRI acquisition

Anatomical and DCE MRI data were acquired using a 3 Tesla MRI system (Achieva TX, Philips Healthcare, Best, the Netherlands) with a 32-channel head coil. The imaging protocol included a 3D T1-weighted inversion recovery fast gradient echo (repetition time (TR) of 8 ms; inversion time (TI) of 800 ms; echo time (TE) of 4 ms; flip angle of 8°; 1 mm cubic voxel size) for anatomic reference; a 3D T2-weighted fluid attenuation inversion recovery (FLAIR) (TR/TI/TE of 4800/1650/290 ms; flip angle of 90°; 1 mm cubic voxel size) for localizing the CVOs; and a dual-time resolution dynamic contrast-enhanced (DCE) MRI acquisition. The dual-time DCE MRI protocol consisted of two nested pulse sequences, a slow and a fast sequence with a saturation recovery preparation pulse, as described earlier (29). In short, the fast sequence used a short dynamic scan interval of 3.2 s during the steep signal changes in initial circulations of the contrast agent, while the slow sequence used a longer interval of 30.5 s during the later extravasation phase when the signal changes are much slower. Before contrast administration (pre-contrast), scans of both sequences were acquired. Subsequently, a bolus injection of gadolinium-based contrast agent was performed during the fast sequence (0.1 mmol/kg gadobutrol, Gadavist®, Bayer AG, Leverkusen, Germany), intravenously in the antecubital vein (injection rate 3 mL/s, 20 mL saline flush). The fast sequence consisted of 29 volumes (TR/TE/delay time (TD) 5.3/2.5/120 ms, voxel size 2 x 2 x 5 mm) and the slow sequence consisted of 30 volumes (TR/TE/TD 5.6/2.5/120 ms, voxel size 1 x 1 x 2 mm). To minimize partial volume, fold over, and inflow effects (of the sagittal sinus superior), an odd number of sagittal orientated slices, 11 for the fast sequence and 75 for the slow sequence, was acquired with the frequency-encoding direction in the craniocaudal direction. T1-mapping with variable delay time settings was performed prior to contrast administration and DCE imaging to enable the conversion of the contrast-enhanced tissue signal intensities to contrast agent concentrations (30).

2.3. Brain regions of interest

One researcher (I.C.M.V.) was trained by an experienced neuroradiologist (A.A.P.) in determining the locations of the CVOs on the basis of brain anatomy from the mid-sagittal anatomical FLAIR images. Recognizable anatomical identification marks were used to determine the location of each CVO (e.g. the hypophysis and mammillary body for the NH and ME; the anterior commissure for the OVLT; the hippocampus and fornix for the SFO; the fourth ventricle for the AP), and a limited number of voxels on this exact location was selected, which were saved as region-of-interest (ROI).

Additionally, a ROI was placed in the nec_k muscle, to observe the temporal enhancement time curves for qualitative comparisons of the contrast agent distribution. As quantitative control, the white and gray matter regions were selected, which were segmented using automated software (FreeSurfer, version 6.0.0

(31)). The FreeSurfer segmentation was visually checked by one researcher (I.C.M.V.) with manual adjustments. From the segmented brain regions, the total gray matter (including cortical gray matter, deep gray matter (thalamus, caudate nucleus, putamen, pallidum, amygdala, and accumbens area), and hippocampus) and total white matter volume were extracted (31).

2.4. Pre-processing

The slow and fast dynamic series were motion corrected and spatially aligned using a linear registration procedure with six degrees of freedom (FLIRT, FMRIB's linear registration tool), with the average pre-contrast slow volume as reference. Next, the motion-corrected dynamic series, the FLAIR images and tissue masks, and T_{10}-map were subsequently registered onto the participant's structural T1-weighted images.

Individual vascular input functions (VIFs) were extracted from manually (I.C.M.V.) selected voxels (≥20) in the superior sagittal sinus (32, 33). Conversion of MRI signal enhancement to contrast agent concentration was performed differently for the VIF and tissue, and has been described earlier in detail (34). In short, the VIF signal-to-concentration conversion was implemented using in vitro data (diluted $MnCl_2$ stock solution with different gadobutrol concentrations (1-40 mM), baseline T1 relaxation time of 1650 ms, comparable to human blood), whereas the conversion to contrast agent concentration in tissue was performed assuming a linear relationship and a tissue relaxation time calculated from the T_{10}-map. Representative contrast agent concentration maps pre- and post-contrast agent injection are shown in Figure 3. A video of the dynamic contrast agent concentration maps during the whole DCE MRI sequence is included as Additional file 2.

2.5. Pharmacokinetic modeling

The CVOs are the points of communication between the blood plasma and the brain tissue and their functionality involves extensive exchange with the blood circulation comprising influx and reflux of solutes (4, 6). To take both the influx and reflux into account, we applied the extended Tofts model (ETM) to the CVO data, which is a two-compartmental model with a blood compartment and an interstitial compartment with bidirectional transport between these compartments (35). The CVOs are expected have a high permeability due to the lack of a blood-brain barrier and thus a sufficiently high signal-to-noise ratio. Therefore, the ROI averaged concentration-time data per CVO were fitted using the ETM as implemented in ROCKETSHIP (36) (fitting parameters for K^{trans}: starting value of 0.001 min^{-1}; lower and upper bound value of -2 and 2 min^{-1}; maximum number of iterations of 50; and a function tolerance of 10^{-12}) to obtain K^{trans} [min^{-1}], the transfer constant from blood plasma to extracellular, extravascular space as measure of permeability, v_p [-], the volume fraction of blood plasma within a ROI as measure of perfusion, and v_e [-], extravascular space volume fraction as a measure of uptake capacity and retention, for each CVO. The ETM provided sufficiently good fits for both secretory and sensory CVOs (Figure 4).

Next, to check whether the ETM sufficiently fitted the CVO data, each fit was visually checked (I.C.M.V.) and rated as ‘good’, ‘doutbful’ or ‘bad’, based on how well the modeled curve matched the data points and whether the time-course of the contrast-enhancement curve was sensible (Table 2).

The graphical Patlak method was used to calculate the leakage rate (influx) of the contrast agent into the interstitial space of the white and gray matter. This method assumes no reflux from the brain back to the blood and has been demonstrated to be most suitable for assessing pharmacokinetic parameters of normal-appearing brain tissue (37). Therefore, we applied the graphical Patlak method to assess K^{trans} [min^{-1}] and v_p [-] in each voxel in the white matter and gray matter. As not in all voxels significant transfer from blood to brain could be measured due to low K^{trans} values in combination with the strong influence of noise, histograms of the K^{trans} values in the white and gray matter were created. These histograms were subsequently corrected for noise (19), after which the mean K^{trans} was calculated as a representative measure for the permeability in the whole white and gray matter region. This approach has been applied previously in healthy controls (19). For the CVOs, the graphical Patlak method did not appear to be best suitable, as due to their exchange function, reflux must also be taken into account for these structures.

In addition to pharmacokinetic analyses, one- and ten-minute areas under the curve (AUCs) [mM·min] were calculated as proxies of gadolinium-based contrast agent wash-in during the circulation phase, and retention during the accumulation phase, respectively. Contrary to the pharmacokinetic parameter, the AUC is not dependent on the type of pharmacokinetic analysis applied and can serve as a data-driven, thus model-free, approach for characterization of contrast enhancement.

2.6. Statistics

To ensure that the transfer constant (K^{trans}) of the CVOs gave a realistic representation of the data, the analyses were performed excluding the values obtained from fits that were classified as ‘bad’. Post-hoc, the analyses were repeated also excluding any fits for which it could be doubted whether they were sufficiently good, to see if this would change the results.

Since our participant sample was relatively small and the transfer constants were not normally distributed for each ROI, non-parametric tests were conducted (Part 1: Wilcoxon signed-rank test; Part 2: Mann-Whitney test). All statistical analyses used a level of significance of $p<0.05$, and were performed with commercial software (SPSS , version 24.0, IBM Corp., Armonk, NY, USA).

2.6.1. Part 1:transfer constants of the CVOs and normal-appearing brain matter

We expected the CVOs to have strong contrast enhancement and significantly positive transfer constants, so a transfer constant significantly higher than 0.

The transfer constants and AUCs were calculated for all CVOs separately, but also for all secretory CVOs combined and all sensory CVOs combined. The Wilcoxon signed-rank test was conducted, comparing the K^{trans} in the secretory and sensory CVOs to a hypothesized median of 0. If a significant result was obtained, post-hoc analyses were conducted to see which specific CVOs were significantly different from 0.

As additional analyses, Wilcoxon signed-rank tests were used to compare the K^{trans} between the secretory and sensory CVOs, and between the CVOs and the white and gray matter. Again, a significant result was followed by post-hoc analyses to determine which specific CVOs had a significantly different permeability from the other CVOs, or from the white or gray matter.

2.6.2. Part 2: Age differences

For the second part, we investigate whether the transfer constant (K^{trans}) differed between the older and middle-aged group.

For this between-subjects test, the Mann-Whitney test was used and the difference between the older and middle-aged group was assessed within the combined secretory CVOs, combined sensory CVOs, white matter and gray matter. If a significant result was obtained for either the combined secretory or sensory CVOs, post-hoc analyses were conducted to see for which specific CVOs the age groups differed most strongly.

3. Results

3.1. Concentration curves of different tissue types

We depicted the temporal enhancement profile in CVO tissue and normal-appearing brain matter, as well as muscle tissue (Figure 5). In the neck muscle tissue, gadolinium-based contrast agent concentration steadily increased (dotted green line). However, the CVO concentration time curves displayed a steep peak followed by gradual decline, which are features also seen in the white and gray matter concentration curves. In this typical pattern, the contrast first quickly circulates through the brain, followed by a slow spread (dispersion). The concentration curves of the secretory CVOs ME and PG showed less steep decline after the initial circulation peaks than the concentration curve of the VIF (Figure 5C), which is indicative of retention of contrast medium in the CVOs. For the secretory NH structure, retention is also visible by a broadening (hump) after the initial peak (Figure 5C).

3.2. Transfer constants of the CVOs

For the secretory CVOs, significantly positive transfer constants (K^{trans}) were found ($p < .001$; Table 2). Post-hoc analyses revealed that this was the case for all secretory CVOs (NH, ME and PG; all p values £ .001).

Also in the sensory CVOs, significantly positive transfer constants were found ($p = .007$; Table 2). Post-hoc analyses revealed that this was the case for the OVLT and AP (all p values £ .007), but not for the SFO ($p = .208$). The SFO was also the organ for which the least good fits were obtained ($n = 8$), with a lower permeability possibly making the data more susceptible to noise and therefore harder to estimate.

Repeating the analyses while also excluding the cases for which the goodness of fit could be doubted, did not change the results.

The values for the blood plasma fraction (v_p) and the interstitial space fraction (v_e) can be found in Additional file 3.

Table 2. The median and interquartile range (25^{th} – 75^{th} percentile) of the transfer constant (K^{trans}) and the number of good fits measured in various regions-of-interest (ROIs).

ROI	**ETM K^{trans} [min^{-1}]**	**25^{th} – 75^{th} percentile**	**Number of good fits from a total of 20**
Secretory	**.22***	.17 – .33	**19**
NH	.40*	.29 – .63	19
ME	.048*	.032 – .11	19
PG	.078*	.033 – .12	16
Sensory	**.026***	.021 – .036	**10**
SFO	$1.8 \cdot 10^{-3}$	$-.69 \cdot 10^{-3}$ – $25 \cdot 10^{-3}$	8
OVLT	.019*	.0091 – .034	17
AP	$10 \cdot 10^{-3}$*	$.87 \cdot 10^{-3}$ – $80 \cdot 10^{-3}$	10
	Patlak K^{trans} [min^{-1}]		
White matter	$4.1 \cdot 10^{-7}$*	$.52 \cdot 10^{-7}$ – $9.3 \cdot 10^{-7}$	N.A.†
Gray matter	$13 \cdot 10^{-7}$*	$5.1 \cdot 10^{-7}$ – $17 \cdot 10^{-7}$	N.A.†

Abbreviations: NH = neurohypophysis; ME = median eminence; PG = pineal gland; SFO = subfornical organ; OVLT = organum vasculosum of the lamina terminalis; AP = area postrema

* K^{trans} significantly larger than 0 ($p<.05$)

† Goodness of fit not applicable as a voxelwise Patlak method followed by noise correction using histrogram approach was used

3.3. Transfer constants in the secretory CVOs compared to the sensory CVOs

The secretory CVOs had higher transfer constants than the sensory structures ($p < .001$). Even comparing the secretory CVO with the lowest K^{trans} (ME) to the sensory CVO with the highest K^{trans} (OVLT), revealed that the ME still had a significantly higher transfer constant than the OVLT ($p = .014$), so all secretory CVOs had significantly higher transfer constants than each sensory CVO.

3.4. Transfer constants in the CVOs compared to the normal-appearing brain matter

Comparing the CVOs to the white and gray matter gave results comparable to the main analyses, with the transfer constants being significantly larger in the CVOs than in the white matter and gray matter (all p values £ .004), except for the SFO (both p values = .250).

The model-independent check with AUC values also found stronger contrast enhancement in the CVOs than in the white matter, but only for the secretory structures, which also had the highest permeability parameters when applying the pharmacokinetic analysis. The NH was the only structure that showed significantly stronger contrast enhancement than the gray matter.

Comparing the AUCs of the secretory and sensory CVOs gave the same results as comparing the transfer constants, with the secretory CVOs having significantly stronger contrast enhancement than the sensory CVOs.

These results can be found in Additional file 4.

3.5. Age effect

We found no significant differences in transfer constants between the older and middle-aged group in the secretory CVOs and white matter (all p values ³ .549). The age effect did approach significance in the sensory CVOs (older: n = 6, middle-aged: n = 4; p = .067), with the older group tending towards a lower

permeability, and gray matter (older: n = 10, middle-aged: n = 10; p = .051), with the older group tending towards a higher permeability.

Repeating the analyses while also excluding any fits for which it could be doubted whether they were sufficiently good, gave a significant difference for the sensory CVOs (older: n = 5, middle-aged: n = 4; p = .032), with the older group having significantly lower permeability than the middle-aged group.

4. Discussion

4.1. Main findings

In this study, we investigated the feasibility of applying dual-time resolution DCE MRI with a gadolinium-based contrast agent and pharmacokinetic modeling to assess permeability of the CVOs. It was possible to measure gadolinium-based contrast enhancement in these small structures and successfully modeled the temporal uptake curves and derived the influx rate in terms of the transfer constant. Our results demonstrated that positive transfer constants, which were significantly higher than those of the white and gray matter, could be measured in all CVOs, exept for the SFO. Moreover, the transfer constants for the secretory CVOs were significantly higher than for the sensory CVOs. We could not demonstrate any clear significant pharmacokinetic differences in any of the CVOs between the age groups.

4.2. Stronger contrast enhancement in the secretory CVOs

Due to absence of the BBB in the highly fenestrated capillaries, all CVOs were expected to have significantly positive transfer constants, and our results confirmed this hypothesis. The secretory CVOs, and especially the NH as largest peptide-releasing structure, had significantly stronger contrast enhancement and higher transfer constants.

The secretory CVOs being more permeable than the sensory type is supported by previous neurobiological studies. A study in mice previously found higher vascular permeability values in the secretory CVOs relative to the sensory CVOs when using low-molecular-weight contrast agents (fluorescein isothiocyanate (FITC), molecular weight = 0.39 kDa, and Evans Blue, molecular weight = 0.96 kDa), which the researchers attributed to large secretion of peptides into the blood circulation by secretory CVOs (24). Moreover, a follow-up mice study found evidence that astrocyte-tanycyte connections possibly form an alternative barrier in the sensory CVOs (38). In the human brain, post-contrast gadolinium studies were conducted to assess CVO visibility (5, 18). The presence of contrast enhancement in the CVOs on post-contrast T1-weighted 3 Tesla MRI was assessed, as the CVOs were speculated to be mistaken for pathology-related abnormal contrast enhancement (5). The ME, NH and PG were visible in 100%, 96% and 84% of the cases, respectively. The OVLT was visible in 34% of the cases, while the AP and SFO were hardly ever visualized (2% and 1%, respectively) (5). A similar study using post-contrast 3D T2-weighted FLAIR 3T MRI images had comparable outcomes (18). The results of the current study correspond to the results of these previous studies.

The stronger contrast enhancement in the secretory and weaker enhancement in the sensory CVOs found in our study could also have alternative explanations. Blood flow in the sensory CVOs is slower relative to the rest of the brain, for the blood plasma to have better access to the receptors (4). With slower blood flow, less contrast agent may reach the sensory CVOs.

Another confounding factor could be partial volume effects, due to the small size of the structures compared to the voxel sizes of MRI. The CVOs that seem to have the highest transfer constants, the NH and PG, are also the CVOs in close proximity to large vessels with strong contrast enhancement. Partial volume effects of these large vessels might contribute to the high transfer constants found in these CVOs. The presence of a large vessel in the ROI is reflected by obtaining a higher blood plasma volume (Additional file 3, Table 3.1). The ME, which does not seem to lie close to a large vessel, still has a higher transfer constant than the sensory CVOs. Moreover, an extra check in which the transfer constants were calculated for ROIs with a smiliar proximity to the large vessels, but not containing any CVO tissue, resulted in lower transfer constants compared to the values found for the secretory CVO ROIs. Therefore, while partial volume effects from the large vessels might influence the transfer constants, this demonstrates that these effects cannot fully account for the higher transfer rates found in the secretory CVOs. The sensory CVOs, being smaller than the NH and PG (Table 1 (2)), may experience stronger partial volume effects from the surrounding brain tissue. Due to these partial volume effects, measurements in the sensory CVOs could represent an underestimation. To really understand to what extent partial volume effects from large vessels or surrounding tissue influence the results, more in depth research is necessary. To address the influence of partial volume effects, optimizing the technique with a higher spatial resolution by using ultra-high-field MRI, or applying a more sophisticated pharmacokinetic model controlling for cerebral blood flow in each ROI (39), could be an interesting methodological improvement for future studies.

4.3. Age effect

We expected that the CVOs would have less contrast enhancement in the older group, due to a decrease in blood flow. We did not find a clear significant difference in permeability when comparing the older and middle-aged group. A decrease in blood flow could possibly decrease contrast uptake, but it remains unknown whether blood flow is sufficiently reduced in the older subpopulation to display such an effect. Also, age-related vascular alterations might increase permeability (40) and compensate for the reduced blood flow effect.

The age effect did approach significance in the sensory CVOs ($p = .067$) and gray matter ($p = .051$). In the older group, the sensory CVOs tended to be less permeable, suggesting that these structures might be more susceptible to age-related blood flow reduction decreasing permeability. In the gray matter, however, the older group showed a trend towards higher permeability, indicating that this tissue type is more susceptible to age-related vascular alterations increasing permeability, as previous studies have

demonstrated (41, 42). However, it is important to note that the result for the sensory CVOs is based on very small group sizes (older: n = 6, middle-aged: n = 4), and therefore needs further confirmation.

The difficulty to detect a clear age effect could also be because the participants selected from the MAAS study might represent a relatively healthy subsample of the general population, i.e. long-lasting study participants representing 'survivors' in an above-average health state. As any age effect is expected to be subtle in such a subsample, it may well be that our study with 10 participants in each group had insufficient power to detect this effect. Especially in the sensory CVOs, exclusion of 'bad' fits lead to very small sample sizes, and based on the current study we cannot make any definite claims about the presence of an age effect.

4.4. Additional considerations

We used the ETM to model the CVO time-courses, as, from a theoretical perspective, this model seemed most suitable to the CVOs (blood compartment and interstitial compartment with bidirectional exchange between these compartments (35)), and gave the best fit to our data. However, the ETM can only be used in case of weak vascularization or high perfusion (43, 44). In tissues with either high vascularization or very slow or very fast exchange, the ETM can still give a good fit to the data, but the derived pharmacokinetic parameters can be unreliable (44). Therefore, without the certainty that the tissue has either low vascularization or high perfusion, the interpretation of the pharmacokinetic parameters can be misleading. Cerebral tissue is in general highly perfused (45). For the white and gray matter, for instance, the Patlak method has been established to be the preferred model (37), and this model is also intended for highly perfused tissues (43).The Patlak method is not suitable for the CVOs though, due to the added assumption of no reflux from the brain back to the blood, which is violated in the CVOs with their exchange function. Therefore, we feel that the application of the ETM to the CVO data was justified (44).

While we applied the ETM to each CVO ROI, an alternative approach would be voxel-by-voxel model selection (46). According to this approach, when a higher-order model is applied (a model with three or four parameters), this model is routinely tested against lower-order models or plausible alternative models of the same order in each voxel (46, 47). The four commonly used models in DCE MRI are the Patlak model (K^{trans} and v_p), the classical Tofts model (TM; K^{trans} and v_e), the extended Tofts model (ETM; K^{trans}, v_p and v_e) and the two-compartmental exchange model (2CXM; K^{trans}, v_p, v_e and F_p (blood plasma flow)) (43). As the Patlak model assumes no reflux and the TM is a one-compartment model with negligible blood volume (35), these models are not adequate as they contradict CVO functionality (4, 6). However, for future studies, it would be interesting to explore the use of voxel-by-voxel model selection and to compare the fits obtained with the ETM and 2CXM, and discern CVO structures from the surrounding tissue based on physiological measures.

We assessed permeability using the gadolinium-based contrast agent gadobutrol. Pathogens, such as prions and amyloid-b, can be found as soluble proteins in the blood (48, 49), but permeability

characteristics for these pathogens are not necessarily similar to those of gadobutrol, as the molecular weight of prion proteins (27-30 kDa (50)) or amyloid-b peptides (4 kDa (51)) is higher than the weight of gadobutrol (0.61 kDa (52)). Immunohistochemistry studies in mice have demonstrated that permeability in the CVOs is size-selective, and have found different results with low-molecular weight (< 10 kDa) and high-molecular-weight (³ 10 kDa) tracers (38, 53, 54). Studies with high-molecular weight contrast agents should be conducted to confirm these findings in vivo in humans.

5. Conclusion

In this study, dual-time resolution DCE MRI was introduced as a possible method to assess CVO permeability. With this method, significantly positive transfer constants could be measured in the CVOs, and the CVOs were shown to have stronger contrast enhancement relative to the normal-appearing brain matter. This observation indicates that current measurements confirm the often-held assumption of highly permeable CVOs, with the secretory CVOs being most permeable. The CVOs are often referred to as ‘windows of the brain’, and pathogens may enter through these windows and trigger an inflammatory response. More advanced ways to assess CVO permeability might eventually help blocking entrance of pathogens, determine factors that disturb homeostasis and possibly contribute to initiatives to overcome neurodegenerative disorders.

6. List Of Abbreviations

2CXM	Two-compartmental exchange model
AD	Alzheimer’s disease
AP	Area postrema
AUC	Area under the curve
BBB	Blood-brain barrier
CNS	Central nervous system
CSF	Cerebrospinal fluid
CVO	Circumventricular organ
DAD	Disabilities Assessment for Dementia
DCE MRI	Dynamic contrast-enhanced magnetic resonance imaging
ETM	Extended Tofts model
FITC	Fluorescein isothiocyanate

FLAIR	Fluid attenuated inversion recovery
HPA	Hypothalamic-adrenal-pituitary
MAAS	Maastricht Aging Study
ME	Median eminence
METC	Medical ethics review committee
MMSE	Mini-Mental State Examination
NH	Neurohypophysis
NRMSE	Normalized root-mean-square error
NWO	Nederlandse Organisatie voor Wetenschappelijk Onderzoek
OVLT	Organum vasculosum of the lamina terminalis
PG	Pineal gland
ROI	Region of interest
SFO	Subfornical organ
TD	Delay time
TE	Echo time
TI	Inversion time
TM	Tofts model
TR	Repetition time
VIF	Vascular input function
WMA	World Medical Association
WMH	White matter hyperintensity

Declarations

Ethics approval and consent to participate

This study was approved by the medical ethics review committee of Maastricht University Medical Center (approval number: METC163050). The study was conducted according to the principles of the World Medical Association (WMA) Declaration of Helsinki (64th WMA General Assembly, Fortaleza, Brazil, October 2013). All participants provided written informed consent beforehand regarding participation.

Consent for publication

All participants provided written informed consent beforehand regarding publication of the data.

Availability of data and materials

The data that support the findings of this study are available on request from the corresponding author [I.C.M.V.]. The data are not publicly available due to their conficential nature.

Competing interests

The authors declare that they have no competing interests.

Funding

This work was supported by the Nederlandse Organisatie voor Wetenschappelijk Onderzoek (NWO) [Personal Grant I.C.M.V. number 406-15-031].

Author's contribution

Inge Verheggen: Conceptualization, Methodology, Formal Analysis, Investigation, Resources, Data Curation, Writing – Original Draft, Writing – Review & Editing, Visualization, Funding Acquisition **Joost de Jong:** Conceptualization, Methodology, Software, Formal Analysis, Data Curation, Writing – Original Draft, Writing – Review & Editing, Visualization **Martin van Boxtel:** Resources, Writing – Review & Editing, Supervision **Alida Postma:** Methodology, Writing – Review & Editing **Frans Verhey:** Writing – Review & Editing, Supervision, Funding Acquisition **Jacobus Jansen:** Conceptualization, Methodology, Writing – Review & Editing **Walter Backes:** Conceptualization, Methodology, Resources, Writing – Review & Editing, Supervision, Funding Acquisition.

Acknowledgements

The authors would like to acknowledge the participants for their contribution to scientific research and give special thanks to Jos M.G.M. Slenter and Jan H. Jungerius for ongoing software, hardware and network support.

References

1. Benarroch EE. Circumventricular organs Receptive and homeostatic functions and clinical implications. Neurology. 2011;77(12):1198-204.

2. Duvernoy HM, Risold P-Y. The circumventricular organs: an atlas of comparative anatomy and vascularization. Brain research reviews. 2007;56(1):119-47.
3. Oldfield BJ, McKinley MJ. Circumventricular organs. The rat nervous system: Elsevier; 2015. p. 315-33.
4. Sisó S, Jeffrey M, González L. Sensory circumventricular organs in health and disease. Acta neuropathologica. 2010;120(6):689-705.
5. Horsburgh A, Massoud TF. The circumventricular organs of the brain: conspicuity on clinical 3T MRI and a review of functional anatomy. Surgical and Radiologic Anatomy. 2013;35(4):343-9.
6. Gross PM, Weindl A, Knigge KM. Peering through the windows of the brain. Journal of Cerebral Blood Flow & Metabolism. 1987;7(6):663-72.
7. Langlet F, Mullier A, Bouret SG, Prevot V, Dehouck B. Tanycyte-like cells form a blood–cerebrospinal fluid barrier in the circumventricular organs of the mouse brain. Journal of Comparative Neurology. 2013;521(15):3389-405.
8. Cameron OG. Visceral brain–body information transfer. NeuroImage. 2009;47(3):787-94.
9. Cottrell GT, Ferguson AV. Sensory circumventricular organs: central roles in integrated autonomic regulation. Regulatory peptides. 2004;117(1):11-23.
10. McKinley MJ. The sensory circumventricular organs of the mammalian brain: subfornical organ, OVLT and area postrema: Springer Science & Business Media; 2003.
11. Li N-C, Lee A, Whitmer RA, Kivipelto M, Lawler E, Kazis LE, et al. Use of angiotensin receptor blockers and risk of dementia in a predominantly male population: prospective cohort analysis. Bmj. 2010;340:b5465.
12. Kristensson K, Nygård M, Bertini G, Bentivoglio M. African trypanosome infections of the nervous system: parasite entry and effects on sleep and synaptic functions. Progress in neurobiology. 2010;91(2):152-71.
13. Steinman L. Elaborate interactions between the immune and nervous systems. Nature immunology. 2004;5(6):575.
14. Buller KM. Circumventricular Organs: Gateways to the Brain Role Of Circumventricular Organs In Pro-Inflammatory Cytokine-Induced Activation Of The Hypothalamic–Pituitary–Adrenal Axis. Clinical and Experimental Pharmacology and Physiology. 2001;28(7):581-9.
15. Swaab DF, Bao A-M, Lucassen PJ. The stress system in the human brain in depression and neurodegeneration. Ageing research reviews. 2005;4(2):141-94.
16. Sisó S, González L, Jeffrey M. Neuroinvasion in prion diseases: the roles of ascending neural infection and blood dissemination. Interdisciplinary perspectives on infectious diseases. 2010;2010.
17. Sisó S, Jeffrey M, González L. Neuroinvasion in sheep transmissible spongiform encephalopathies: the role of the haematogenous route. Neuropathology and applied neurobiology. 2009;35(3):232-46.
18. Azuma M, Hirai T, Kadota Y, Khant ZA, Hattori Y, Kitajima M, et al. Circumventricular organs of human brain visualized on post-contrast 3D fluid-attenuated inversion recovery imaging. Neuroradiology.

2018;60(6):583-90.
19. van de Haar HJ, Burgmans S, Jansen JF, van Osch MJ, van Buchem MA, Muller M, et al. Blood-brain barrier leakage in patients with early Alzheimer disease. Radiology. 2016;281(2):527-35.
20. Renkin EM. Effects of blood flow on diffusion kinetics in isolated, perfused hindlegs of cats: a double circulation hypothesis. American Journal of Physiology-Legacy Content. 1955;183(1):125-36.
21. Crone C. The permeability of capillaries in various organs as determined by use of the 'indicator diffusion'method. Acta physiologica scandinavica. 1963;58(4):292-305.
22. Leenders K, Perani D, Lammertsma A, Heather J, Buckingham P, Jones T, et al. Cerebral blood flow, blood volume and oxygen utilization: normal values and effect of age. Brain. 1990;113(1):27-47.
23. Simmons GE, Suchnicki J, Rak K, Damiano T. MR imaging of the pituitary stalk: size, shape, and enhancement pattern. AJR American journal of roentgenology. 1992;159(2):375-7.
24. Morita S, Miyata S. Different vascular permeability between the sensory and secretory circumventricular organs of adult mouse brain. Cell and tissue research. 2012;349(2):589-603.
25. Jolles J, Houx P, Van Boxtel M, Ponds R. Maastricht aging study: Determinants of cognitive aging: Neuropsych Publishers Maastricht; 1995.
26. Fujisawa S, Tanaka J, Nomura M. Estrogen attenuates the drinking response induced by activation of angiotensinergic pathways from the lateral hypothalamic area to the subfornical organ in female rats. Behavioural brain research. 2001;122(1):33-41.
27. Limonta P, Maggi R, Martini L, Piva F. Role of the subcommissural organ in the control of gonadotrophin secretion in the female rat. Journal of Endocrinology. 1982;95(2):207-13.
28. Wenger T, Leonardelli J. Circadian and cyclic LHRH variations in the organum vasculosum of the lamina terminalis of female and male rats. Neuroendocrinology. 1980;31(5):331-7.
29. van de Haar HJ, Burgmans S, Jansen JF, van Osch MJ, van Buchem MA, Muller M, et al. Blood-Brain Barrier Leakage in Patients with Early Alzheimer Disease. Radiology. 2017;282(2):615.
30. Larsson HB, Courivaud F, Rostrup E, Hansen AE. Measurement of brain perfusion, blood volume, and blood-brain barrier permeability, using dynamic contrast-enhanced T(1)-weighted MRI at 3 tesla. Magn Reson Med. 2009;62(5):1270-81.
31. Fischl B. FreeSurfer. NeuroImage. 2012;62(2):774-81.
32. Jelescu IO, Leppert IR, Narayanan S, Araujo D, Arnold DL, Pike GB. Dual-temporal resolution dynamic contrast-enhanced MRI protocol for blood-brain barrier permeability measurement in enhancing multiple sclerosis lesions. J Magn Reson Imaging. 2011;33(6):1291-300.
33. van de Haar HJ, Jansen JFA, Jeukens C, Burgmans S, van Buchem MA, Muller M, et al. Subtle blood-brain barrier leakage rate and spatial extent: Considerations for dynamic contrast-enhanced MRI. Med Phys. 2017;44(8):4112-25.
34. van de Haar HJ, Jansen JFA, van Osch MJP, van Buchem MA, Muller M, Wong SM, et al. Neurovascular unit impairment in early Alzheimer's disease measured with magnetic resonance imaging. Neurobiol Aging. 2016;45:190-6.

35. Heye AK, Thrippleton MJ, Armitage PA, Valdés Hernández MdC, Makin SD, Glatz A, et al. Tracer kinetic modelling for DCE-MRI quantification of subtle blood–brain barrier permeability. NeuroImage. 2016;125:446-55.
36. Barnes SR, Ng TS, Santa-Maria N, Montagne A, Zlokovic BV, Jacobs RE. ROCKETSHIP: a flexible and modular software tool for the planning, processing and analysis of dynamic MRI studies. BMC medical imaging. 2015;15(1):19.
37. Cramer SP, Larsson HB. Accurate determination of blood–brain barrier permeability using dynamic contrast-enhanced T1-weighted MRI: a simulation and in vivo study on healthy subjects and multiple sclerosis patients. Journal of Cerebral Blood Flow & Metabolism. 2014;34(10):1655-65.
38. Morita S, Furube E, Mannari T, Okuda H, Tatsumi K, Wanaka A, et al. Heterogeneous vascular permeability and alternative diffusion barrier in sensory circumventricular organs of adult mouse brain. Cell and tissue research. 2016;363(2):497-511.
39. Sourbron S, Ingrisch M, Siefert A, Reiser M, Herrmann K. Quantification of cerebral blood flow, cerebral blood volume, and blood–brain-barrier leakage with DCE-MRI. Magnetic Resonance in Medicine: An Official Journal of the International Society for Magnetic Resonance in Medicine. 2009;62(1):205-17.
40. Heiss C, Keymel S, Niesler U, Ziemann J, Kelm M, Kalka C. Impaired progenitor cell activity in age-related endothelial dysfunction. Journal of the American College of Cardiology. 2005;45(9):1441-8.
41. Verheggen IC, de Jong JJ, van Boxtel MP, Gronenschild EH, Palm WM, Postma AA, et al. Increase in blood–brain barrier leakage in healthy, older adults. GeroScience. 2020:1-11.
42. Starr JM, Farrall AJ, Armitage P, McGurn B, Wardlaw J. Blood–brain barrier permeability in Alzheimer's disease: a case–control MRI study. Psychiatry Research: Neuroimaging. 2009;171(3):232-41.
43. Sourbron SP, Buckley DL. Classic models for dynamic contrast-enhanced MRI. NMR in Biomedicine. 2013;26(8):1004-27.
44. Sourbron SP, Buckley DL. On the scope and interpretation of the Tofts models for DCE-MRI. Magnetic resonance in medicine. 2011;66(3):735-45.
45. Detre JA, Zhang W, Roberts DA, Silva AC, Williams DS, Grandis DJ, et al. Tissue specific perfusion imaging using arterial spin labeling. NMR in Biomedicine. 1994;7(1-2):75-82.
46. Ewing JR, Bagher-Ebadian H. Model selection in measures of vascular parameters using dynamic contrast-enhanced MRI: experimental and clinical applications. NMR in Biomedicine. 2013;26(8):1028-41.
47. Donaldson SB, West CM, Davidson SE, Carrington BM, Hutchison G, Jones AP, et al. A comparison of tracer kinetic models for T1-weighted dynamic contrast-enhanced MRI: Application in carcinoma of the cervix. Magnetic Resonance in Medicine. 2010;63(3):691-700.
48. Edgeworth JA, Farmer M, Sicilia A, Tavares P, Beck J, Campbell T, et al. Detection of prion infection in variant Creutzfeldt-Jakob disease: a blood-based assay. The Lancet. 2011;377(9764):487-93.

49. Lue L-F, Guerra A, Walker DG. Amyloid Beta and Tau as Alzheimer's Disease Blood Biomarkers: Promise From New Technologies. Neurol Ther. 2017;6(Suppl 1):25-36.
50. Collinge J. Molecular neurology of prion disease. Journal of Neurology, Neurosurgery & Psychiatry. 2005;76(7):906-19.
51. Chen G-f, Xu T-h, Yan Y, Zhou Y-r, Jiang Y, Melcher K, et al. Amyloid beta: structure, biology and structure-based therapeutic development. Acta Pharmacologica Sinica. 2017;38(9):1205.
52. Gadavist, CID=70678987 [Internet]. U.S. National Library of Medicine. 2019 [cited Nov. 13, 2019]. Available from: https://pubchem.ncbi.nlm.nih.gov/compound/Gadavist.
53. Miyata S. New aspects in fenestrated capillary and tissue dynamics in the sensory circumventricular organs of adult brains. Frontiers in Neuroscience. 2015;9(390).
54. Willis C, Garwood C, Ray D. A size selective vascular barrier in the rat area postrema formed by perivascular macrophages and the extracellular matrix. Neuroscience. 2007;150(2):498-509.

Figures

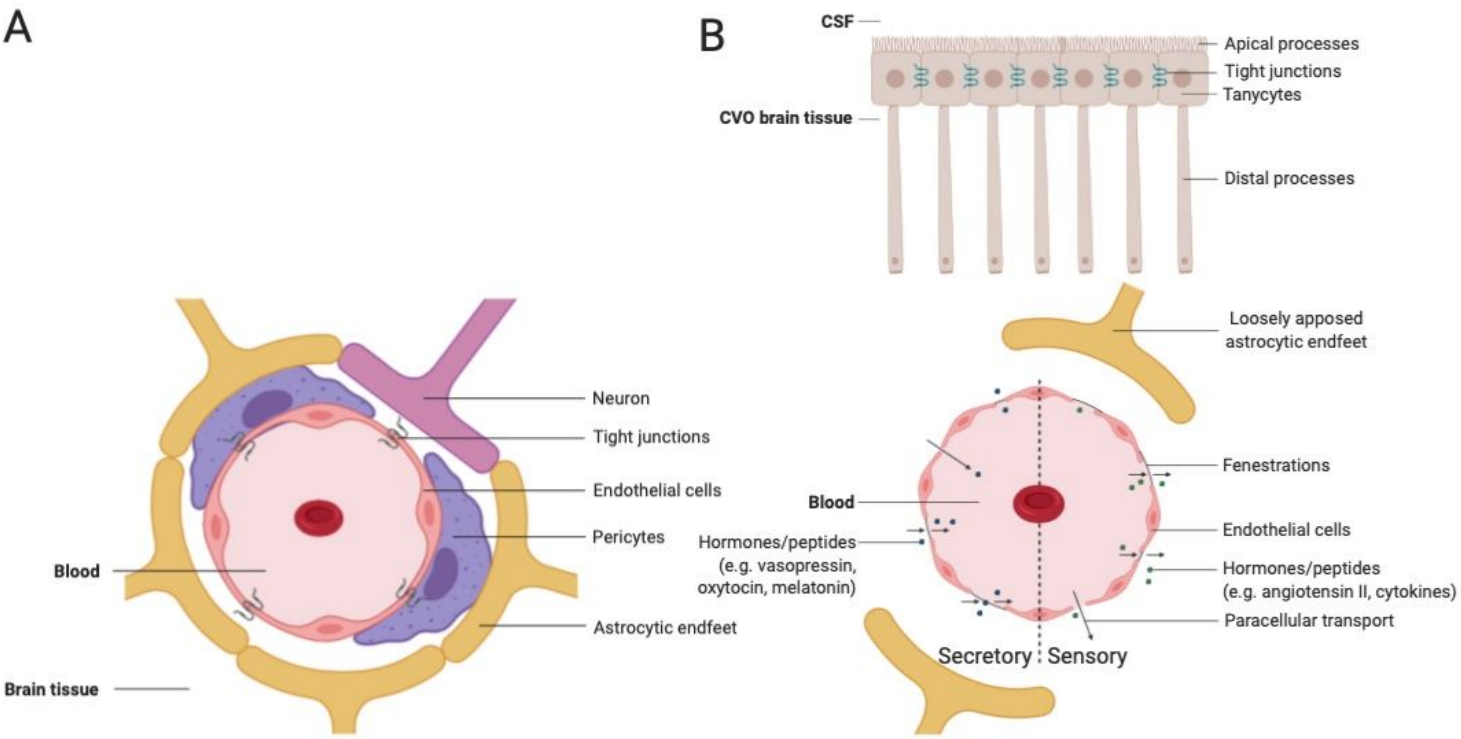

Figure 1

A: cross-section of a blood vessel with a normal blood-brain barrier. B: circumventricular organ with a cross-section of a capillary with a fenestrated endothelium, with on the left half the secretory and on the right half the sensory type. Tanycytes monitor cerebrospinal fluid composition and pass this information to the circumventricular organ. Figure created with BioRender.com.

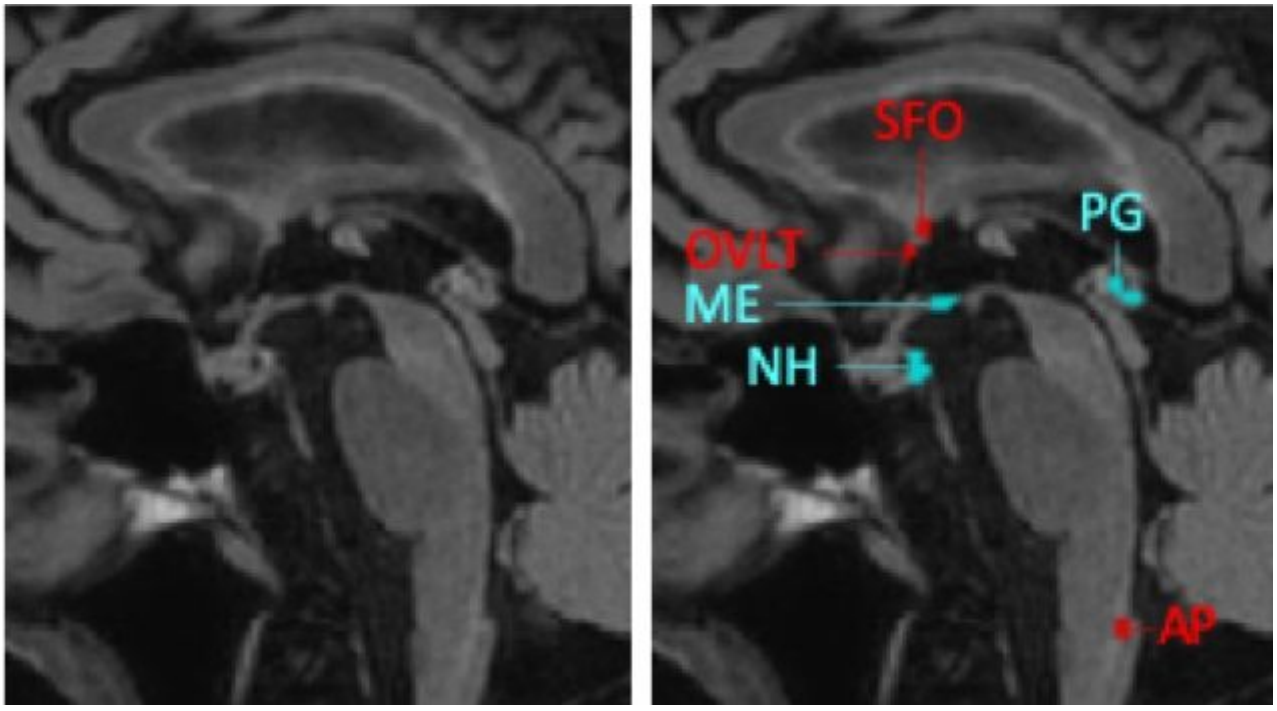

Figure 2

Example of a mid-sagittal anatomical FLAIR image and the regions-of-interest of the secretory (blue) and sensory (red) circumventricular organs. Abbreviations: NH = neurohypophysis, ME = median eminence, PG = pineal gland, SFO = subfornical organ, OVLT = organum vasculosum of the lamina terminalis, AP = area postrema.

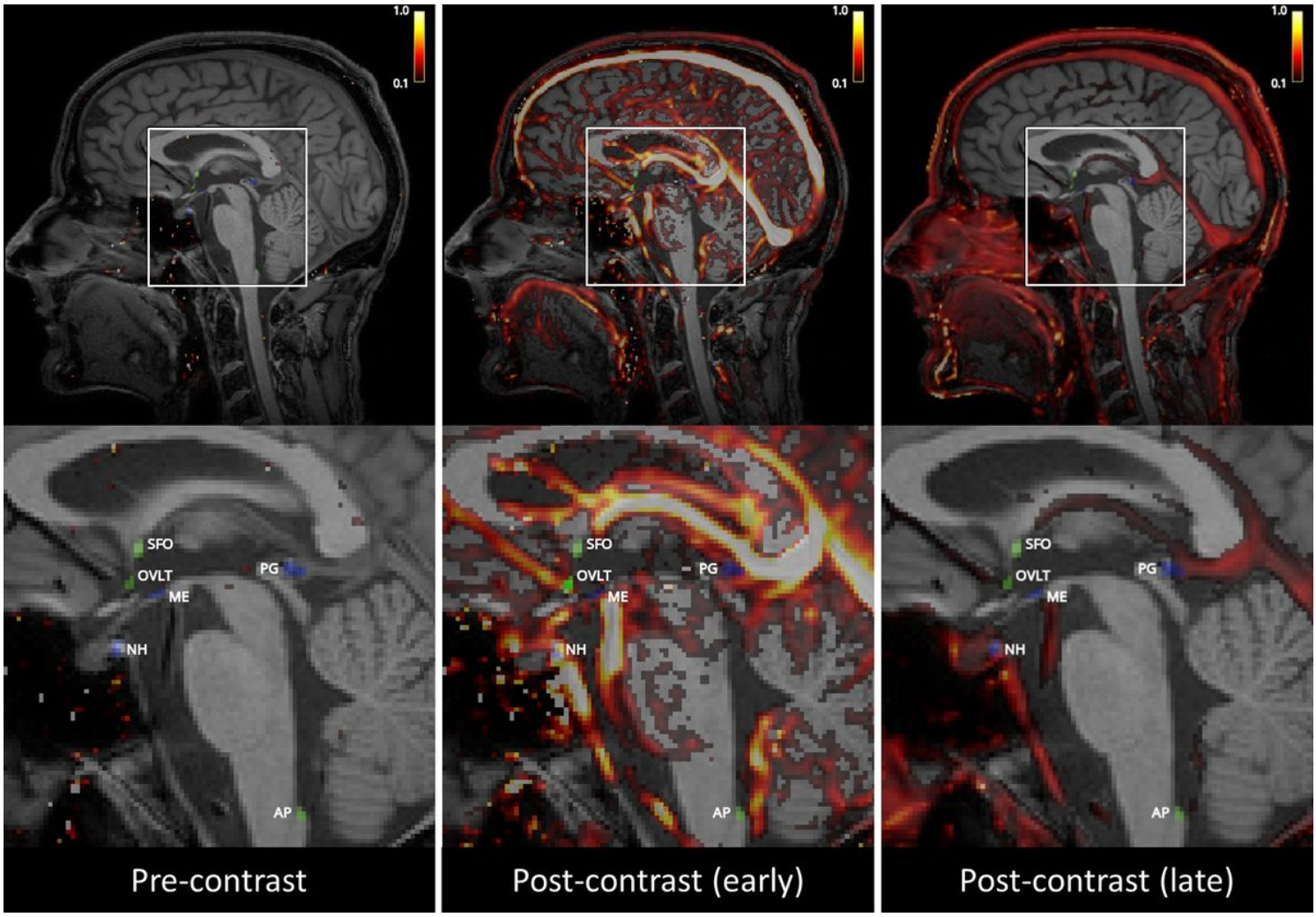

Figure 3

Representative contrast agent concentration maps [mM] showing the distribution of contrast agent before (left), shortly after (middle), and approximately 12 minutes after (right) contrast agent injection.

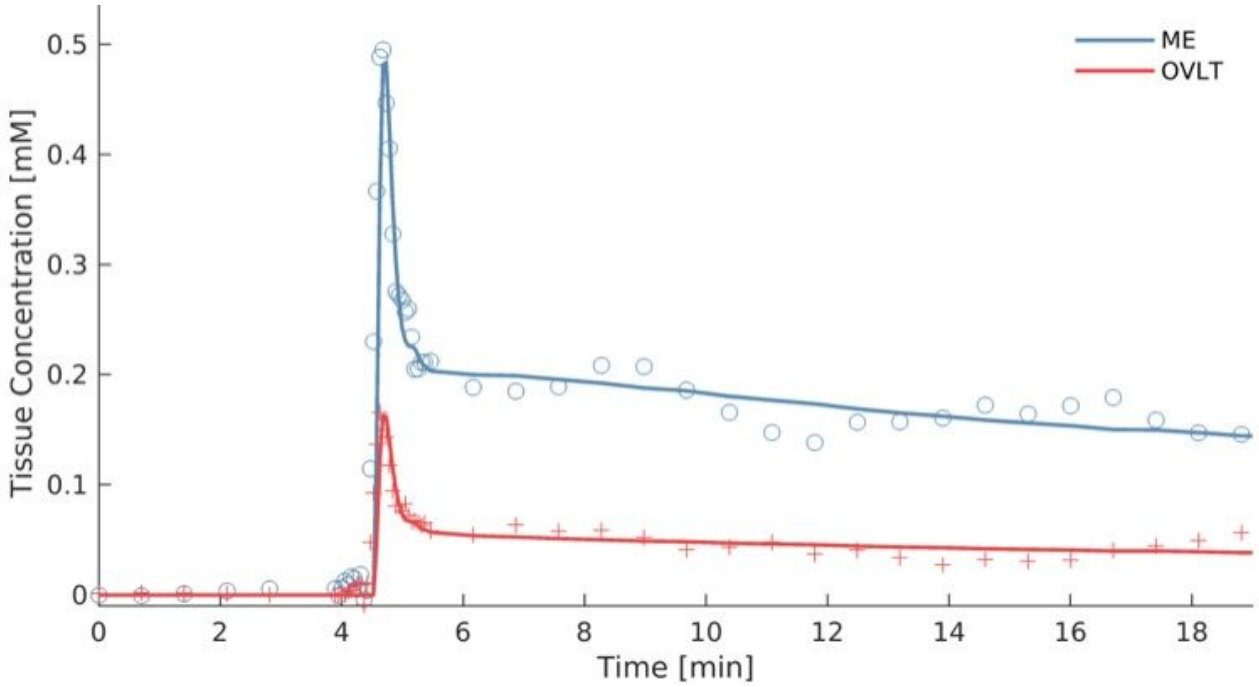

Figure 4

Example of time-concentration curves with good model fits obtained in a secretory (median eminence (ME)) and a sensory (organum vasculosum of the lamina terminalis (OVLT)) circumventricular organ using the extended Tofts model. Note the higher temporal sampling for 1.5 minute during the initial steep concentration changes and the slower sampling before and after this period.

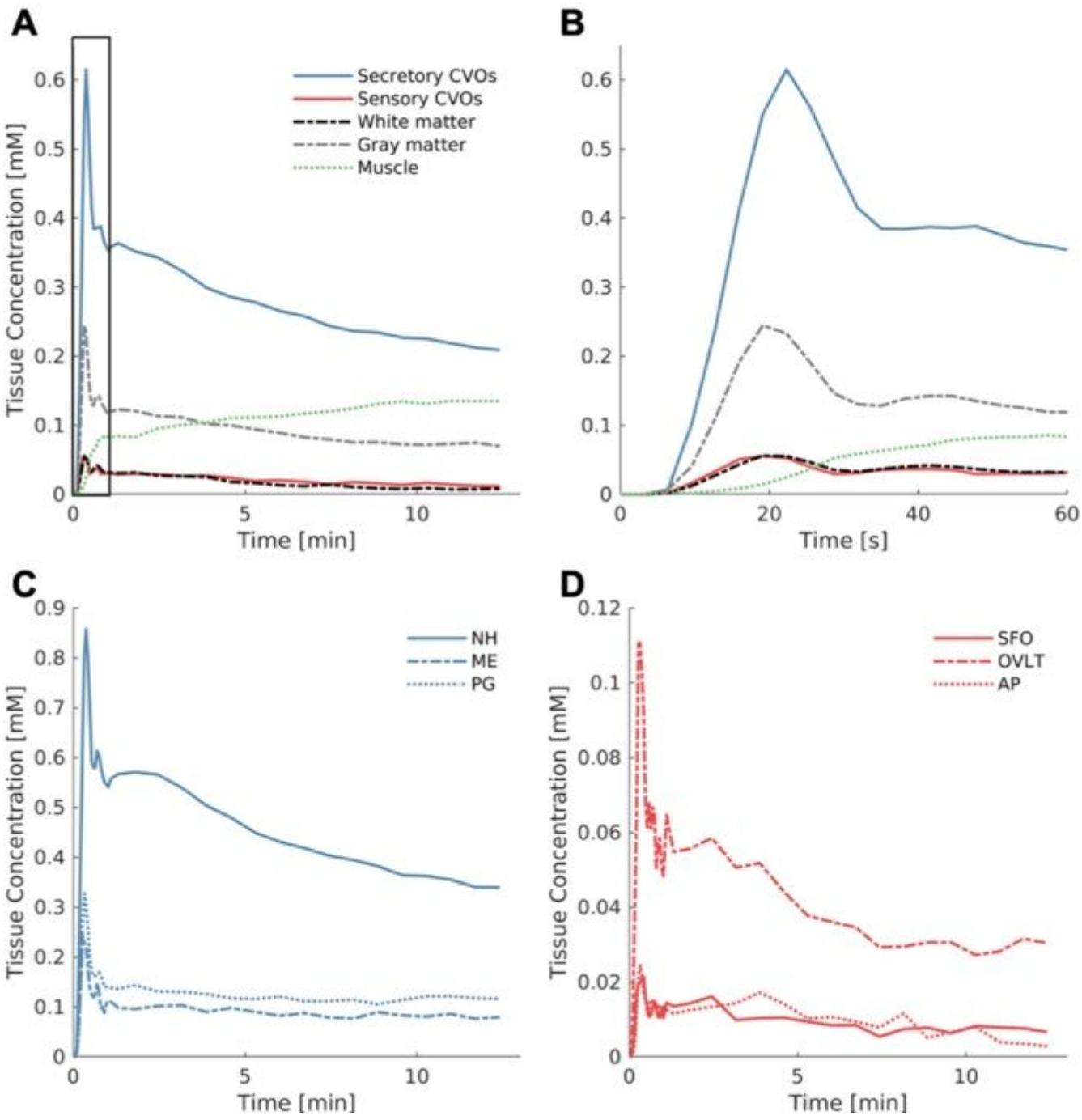

Figure 5

Time course of the gadolinium-based contrast agent concentration in different tissue types and the sagittal sinus (vascular input function (VIF)) averaged over all participants. A and B: In the combined secretory and combined sensory circumventricular organs, white and gray matter and neck muscle since arrival to end of sequence (A) and detailed for the first minute (B); C: In the secretory circumventricular organs neurohypophysis (NH), median eminence (ME) and pineal gland (PG); and D: In the sensory circumventricular organs subfornical organ (SFO), organum vasculosum of the lamina terminalis (OVLT), and area postrema (AP).

Supplementary Files

This is a list of supplementary files associated with this preprint. Click to download.

- FBCNSAdditionalfile1CVOVerheggen.docx
- FBCNSAdditionalfile2VideoCVOVerheggen.mp4
- FBCNSAdditionalfile3CVOVerheggen.docx
- FBCNSAdditionalfile4CVOVerheggen.docx